Available online at www.sciencedirect.com
ScienceDirect
Intermetallics 15 (2007) 1497–1503
Intermetallics
www.elsevier.com/locate/intermet

Interpretation of the morphology and crystallography of precipitate γ_1-$Ti_4Nb_3Al_9$ in $L1_0$-TiAl(Nb)-based intermetallics by invariant line theory

Liu Hong-Wei [a,*], Luo Cheng-Ping [b], Yuan Yong [c], Liu Jun-Ming [d], Liu Zhi-Guo [d]

[a] College of Mechanical Engineering, Guangxi University, Nanning 530004, PR China
[b] School of Mechanic Engineering, South China University of Technology, Guangzhou 510640, PR China
[c] Institute of Solid State Physics, Chinese Academy of Science, Hefei 230031, PR China
[d] National Key Laboratory of Solid State Microstructure, Nanjing University, Nanjing 210093, PR China

Received 29 December 2006; received in revised form 21 February 2007; accepted 28 April 2007
Available online 1 August 2007

Abstract

The coherent precipitate γ_1-$Ti_4Nb_3Al_9$ in the Nb-modified TiAl-based intermetallic compound with a nominal composition of Ti–48 at% Al–10 at% Nb was investigated by transmission electron microscopy. The crystallographic and morphologic characteristics of the precipitating phase have been calculated based on invariant line theory. It is revealed that in the γ-TiAl(Nb)/γ_1-$Ti_4Nb_3Al_9$ couples, both the morphological and crystallographical characteristics of the precipitate γ_1-$Ti_4Nb_3Al_9$ could be predicted by the three-dimensional phase transformation invariant line model. The needle direction of [001] at the early stage for coherent precipitate γ_1-$Ti_4Nb_3Al_9$ and [111] for equilibrium phase γ_1-$Ti_4Nb_3Al_9$ have both been explained well. The characterization of morphology and crystallography of the precipitate reaction in γ-TiAl/γ_1-$Ti_4Nb_3Al_9$ system sustain the postulate that precipitates are bounded by unrotated planes (eigenplanes) when three real eigenvalues exist.

PACS: 71.20.L; 68.37.Lp; 81.40

Keywords: A. Titanium aluminides, based on TiAl; B. Phase transformation; B. Crystallography; F. Electron microscopy, transmission

1. Introduction

Titanium aluminide intermetallic compounds are candidates as high temperature structural materials due to their high specific strength, high melting point and good oxidation resistance at elevated temperature. A lot of research efforts were devoted to this kind of alloys [1–3].

γ-TiAl alloys containing 5–10 at% Nb are regarded as the most perspective high temperature intermetallics. Precipitation behaviors of carbides and silicides in C + Si-alloyed γ-TiAl [4,5] and precipitation behavior of carbides in Ag-modified $L1_2$-Al_3Ti and $L1_0$-TiAl(Ag) [6,7] have been investigated previously. However, to the knowledge of the present authors, precipitation behavior of Nb in high Nb-containing γ-TiAl alloys has not been studied in detail. Hellwig et al. [8] and Chen et al. [9] have reported the diagram of the 1273 K, 1473 K and 1673 K isothermal sections of the Ti–Al–Nb system. Crystallographic structure of the phase $Ti_4Nb_3Al_9$ (γ_1) equilibrium phase was then reported by Chen et al. [10]. The $L1_0$-TiAl phase is of an ordered face-centered tetragonal structure with parameters $a = 0.3976$ nm and $c = 0.4049$ nm. The γ_1-$Ti_4Nb_3Al_9$ phase is tetragonal with lattice parameter a in the range 0.558–0.584 nm and c in the range 0.815–0.845 nm. Its space group is *P4/mmm*. The equilibrium morphology takes needle-like shape with an axis of ⟨111⟩ [11].

We have reported that the γ_1-$Ti_4Nb_3Al_9$ could also precipitate as metastable phase from the γ-TiAl matrix [12]. A detailed transmission electron microscopy (TEM) study was done on the morphological and crystallographical characteristics of γ_1-$Ti_4Nb_3Al_9$ precipitation in the γ-TiAl matrix. The

* Corresponding author. Tel./fax: +86 771 3232294.
E-mail address: hwliu@gxu.edu.cn (L. Hong-Wei).

0966-9795/$ - see front matter © 2007 Published by Elsevier Ltd.
doi:10.1016/j.intermet.2007.04.015

γ_1-$Ti_4Nb_3Al_9$ precipitates, which formed after a normal quench at 1473 K and ageing treatment at 1073 K, were needle-like with a growing axis parallel to [001] direction of the matrix.

The orientation relationship between the γ_1 phase and the γ-TiAl matrix was $[001]_{\gamma_1}//[001]_{\gamma}$, $(100)_{\gamma_1}//(110)_{\gamma}$ and $(010)_{\gamma_1}//(\bar{1}10)_{\gamma}$.

The crystallography and morphologies of products of phase transformations have been the subject of major research for many years. In recent decades, many rival models have been developed to account for orientation relationship (OR), habit plane (HP) and growing orientation of the transforming products. It notably includes phenomenological theory of martensite crystallography [13,14], invariant line strain model [15–17], structural ledges [18], O-lattice [19], Δg parallelism rules [20], edge-to-edge matching [21,22] and planar interphase boundaries migrating mechanism [23], etc. They have been successfully applied to a wide range of transformation products. However, none of them seem to be sufficiently general. Invariant line theory is proved to be effective to those diffusion-controlled phase transformations whose products have a shape of needle, short-bar, platelet and facet, etc [24–26].

The aim of this paper is to make a rational explanation for the morphology and crystallography of γ_1-$Ti_4Nb_3Al_9$ precipitate at the early stage in a $L1_0$-TiAl matrix and for those of γ_1-$Ti_4Nb_3Al_9$ equilibrium phase in $Ti_4Nb_3Al_9$ alloy with three-dimensional invariant line theory. The simple and distinct calculation method of three-dimensional invariant line used here has been reported elsewhere [27], which could allow one to validate completely our calculation process. The needle direction of [001] at early stage for coherent precipitate γ_1-$Ti_4Nb_3Al_9$ and [111] for equilibrium phase γ_1-$Ti_4Nb_3Al_9$ will been explained based on the invariant line theory.

2. Experiments

The material used in this study has a nominal composition of Ti–48Al–10Nb (atom percentage). The alloy was prepared by levitation melting of high purity (99.9%) Ti, Al and Nb in copper crucible under argon atmosphere. Al and Nb are added as interalloy $AlNb_3$. Heart-button ingot of about 200 g was reversed and remelted for three times in order to reduce segregation. Since the weight loss of this melting method is very low, the final alloy composition verified by X-ray Fluorescence spectrometer (XRF) is close to the nominal composition (see Table 1). Then, the alloy ingot was homogenized at 1473 K for 4 h and ageing at 1073 K for 34 h.

The TEM samples were cut into thin slices from the ingots followed by mechanical grinding to about 60 μm thickness. Preparation of discs was carried out using double-jet electropolishing technique with an electrolyte consisting of 65 vol% methanol, 30 vol% butanol and 5 vol% perchloric acid at 30 V and 253 K to 243 K. The foils were examined in a Philips Tecnai F20 transmission electron microscope. High-resolution TEM (HRTEM) investigation was also performed.

Table 1
The nominal and analytical composition of the Ti–48Al–10Nb alloy

	Ti	Al	Nb	Fe	Total
Nominal	42	48	10	0	100
Analytical	43.28	45.10	10.71	0.81	100

3. Results and discussion

3.1. Microstructure and crystallographic characteristics of the Ti–48Al–10Nb alloy

Fig. 1 shows the microstructure of the Ti–48Al–10Nb alloy taken at $[110]_{\gamma}$ (a) and $[001]_{\gamma}$ (c). Fig. 1(b), (c), (e) and (f) are selected area electron diffractions taken down [110]m, [010]m, [001]m, and [013]m, respectively. It is noticed that the diffraction pattern of γ_1-$Ti_4Nb_3Al_9$ does actually overlap on that of γ-TiAl shown in Fig. 1(b) taken down $[110]_{\gamma}//[100]_{\gamma_1}$. This could be revealed by the stereographic projections corresponding to plane (Fig. 1(g)) or corresponding to direction (Fig. 1(h)). It could also be verified by calculating interplanar distances based on the crystallographic parameters of the γ_1-$Ti_4Nb_3Al_9$ and γ-TiAl couple. The Bain orientation relationship between γ_1-$Ti_4Al_3Nb_9$ and $L1_0$-TiAl(Nb) is clearly illustrated by such stereographic projections, i.e., $[001]_{\gamma_1}//[001]_{\gamma}$, $(100)_{\gamma_1}//(110)_{\gamma}$ and $(010)_{\gamma_1}//(\bar{1}10)_{\gamma}$.

The microstructure of the alloy consists of matrix and needle-like precipitates. The EDP and composition analysis as we have done in our previous study [12] confirmed that the matrix is γ-TiAl(Nb) with $L1_0$ structure and the precipitates are γ_1-$Ti_4Al_3Nb_9$ with orthorhombic structure. The γ_1-$Ti_4Al_3Nb_9$ precipitates (denoted as "p") nucleate in the $L1_0$ matrix (denoted as "m") homogeneously adopting a needle-like shape with growing orientation $[001]_{\gamma_1}//[001]_{\gamma}$, a habit plane of $(110)_m$ and a Bain orientation relationship ($[001]_{\gamma_1}//[001]_{\gamma}$, $(100)_{\gamma_1}//(110)_{\gamma}$ and $(010)_{\gamma_1}//(\bar{1}10)_{\gamma}$) with the matrix. Fig. 2 is a high-resolution TEM (HRTEM) image showing the lattice corresponding between the precipitate and the matrix viewed at $[010]_{\gamma}$. Inset is an inverse fast Fourier transition (IFFT) image down $[001]_{\gamma}$, from which the cross-section of the precipitate phase is revealed to take as quadratic form and the precipitate was bounded by planes $(100)_{\gamma_1}//(110)_{\gamma}$ and $(010)_{\gamma_1}//(\bar{1}10)_{\gamma}$ which indicated the precipitate took a parallelepiped shape. Notice the IFFT image was taken from our previous work [12] for further discussing the morphology. The original HRTEM image is corresponding to Fig. 7 in literature [12].

3.2. Morphology and crystallography of the γ_1-$Ti_4Al_3Nb_9$ precipitating phase

3.2.1. Lattice transformation and deformation

As mentioned above, invariant line theory is proved to be effective to those diffusion-controlled phase transformations whose products have a shape of needle, short-bar, platelet and facet, etc. For a phase transformation system of γ_1-$Ti_4Al_3Nb_9$ (precipitate, tetragonal (T))/$L1_0$-TiAl(Nb) (matrix, face-centered tetragonal (FCT)), the lattice correspondence can be regarded as type of FCT to body-centered tetragonal (BCT)

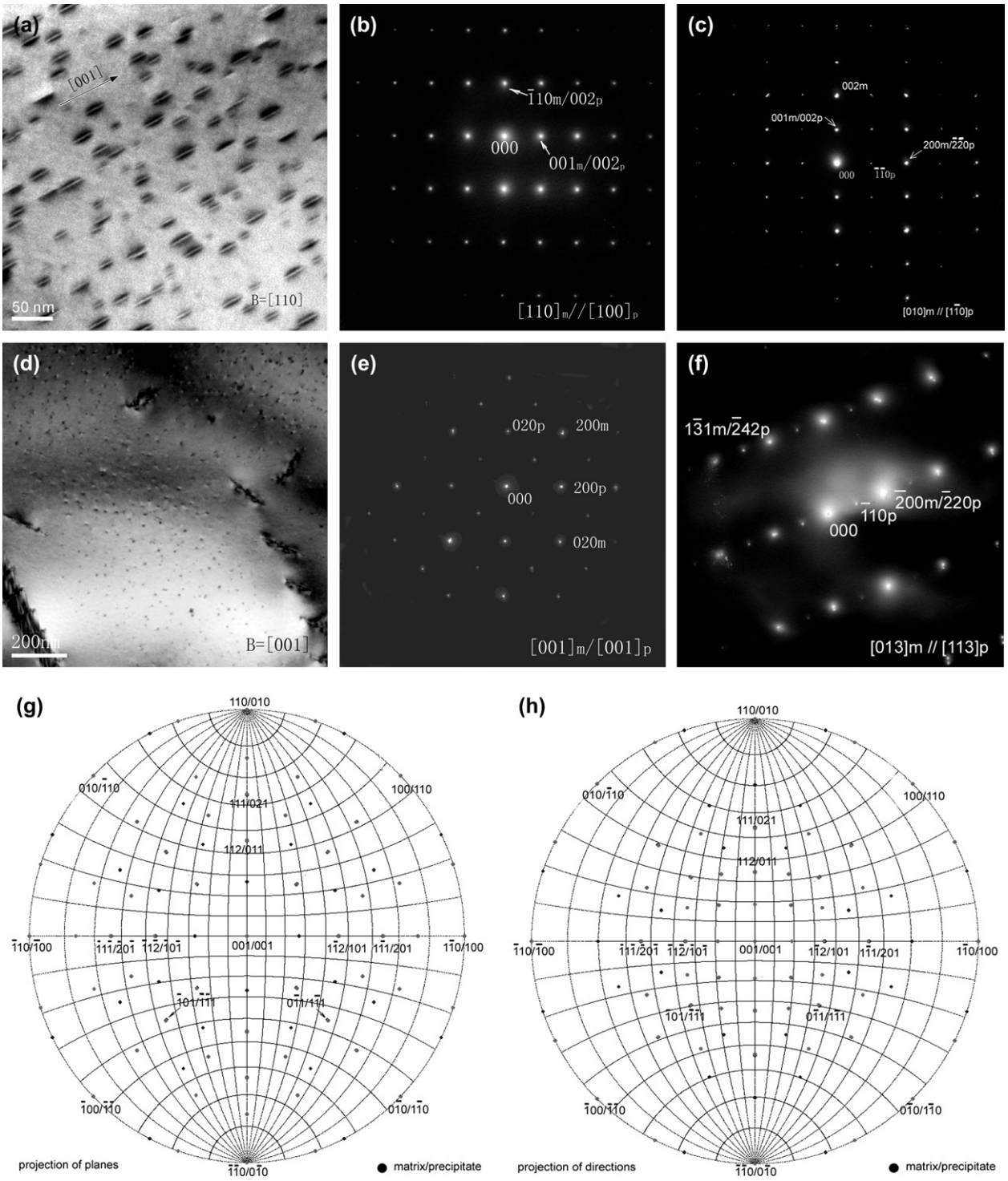

Fig. 1. The microstructures of the Ti-48 at% Al-0 at% Nb alloy taken at $[110]_m$ (a) and $[001]_m$ (d). Notice the needle-like projection morphology of precipitates in (a) and spot-like projection morphology of precipitates in (d); (b), (c), (e) and (f) are selected area electron diffractions taken down $[110]_m$, $[010]_m$, $[001]_m$, and $[013]_m$, respectively; (g) and (h) are stereographic projections of planes (g) and of directions (h) showing the orientation relationship between the matrix and the precipitate, pole center is $[001]_\gamma/[001]_{\gamma_1}$.

based on the fact that the unit cell of the phase γ_1-$Ti_4Al_3Nb_9$ contains eight small BCT cells [10] shown in Fig. 3(a). Crystal structure of the γ-TiAl matrix is shown in Fig. 3(b). Fig. 4 shows a simple lattice corresponding model of Bain strain of FCT/BCT system. The coordinate system is also denoted. The main strain is denoted with η_i (the subscripts "m" and "p" mean matrix and precipitate, respectively). The generalized Bain deformation (the parameters takes $a_m = 0.3976$ nm, $c_m = 0.4051$ nm for γ-TiAl and $a_p = 0.58$ nm, $c_p = 0.81$ nm for γ_1-$Ti_4Al_3Nb_9$) can be expressed as:

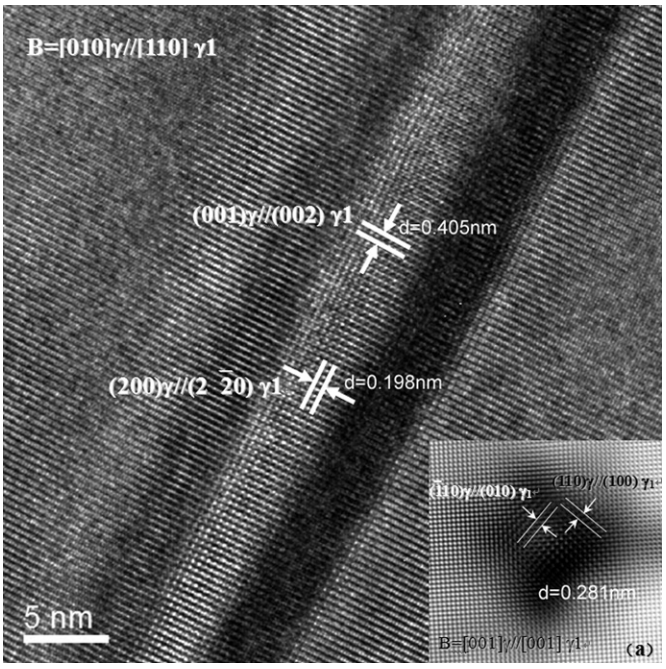

Fig. 2. The HRTEM image of the precipitate viewed at $[010]_{\gamma}//[100]_{\gamma_1}$; in-set (a) shows an IFFT image of the precipitate viewed at $[001]_{\gamma}//[001]_{\gamma_1}$.

$$B=\begin{pmatrix}\eta_1 & 0 & 0\\ 0 & \eta_2 & 0\\ 0 & 0 & \eta_3\end{pmatrix}=\begin{pmatrix}\frac{a_p/2}{a_m/\sqrt{2}} & 0 & 0\\ 0 & \frac{a_p/2}{a_m/\sqrt{2}} & 0\\ 0 & 0 & \frac{c_p/2}{c_m}\end{pmatrix}=\begin{pmatrix}1.03149 & 0 & 0\\ 0 & 1.03149 & 0\\ 0 & 0 & 0.99975\end{pmatrix} \quad (1)$$

After lattice deformation, crystallographic orientation relationship (O.R.) between the matrix and the precipitate can be expressed as:

$$\begin{aligned}&(001)_m//(001)_p;\\ &[110]_m//[100]_p;\\ &[\bar{1}10]_m//[100]_p;\end{aligned} \quad (2)$$

It is obviously that this orientation relationship is typical Bain relationship.

3.2.2. Rigid-body rotation

Based on the invariant line strain model, one or several rigid-body rotations of the new phase may occur with respect to the matrix in order to reach the best orientation relationship (or the best matching) after lattice deformation. In this study, the precipitating phase needs one step rotation to get the phase transformation invariant line.

This step is to let the lattice of precipitating phase to rotate an angle of θ around X axis (the X axis in the reference coordinate system), and the rotation matrix R is easy to take out after Wayman's results [28]:

$$R=\begin{pmatrix}1 & 0 & 0\\ 0 & \cos\theta & -\sin\theta\\ 0 & \sin\theta & \cos\theta\end{pmatrix} \quad (3)$$

According to the determination of the invariant line strain, the calculated rotation angle is 0.18°. In this system, one step rotation is enough to realize invariant line strain. This will lead to an invariant line becoming reality and to define an orientation relationship between the precipitate and matrix.

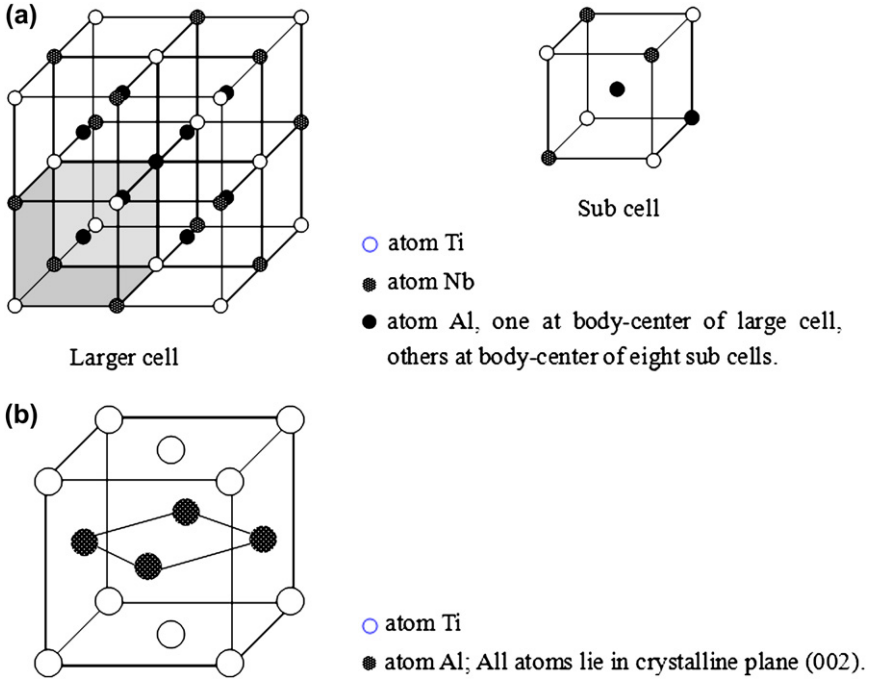

Fig. 3. Crystal structures of γ1-$Ti_4Nb_3Al_9$ (a) and γ-TiAl (b).

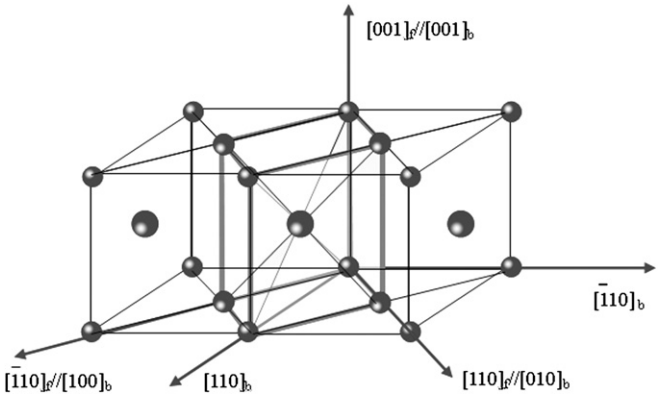

Fig. 4. A schematic showing the lattice rearrangement of FCT-to-BCT transformation.

3.2.3. Calculation of invariant line

The phase transformation invariant line deformation A is:

$$A = RB = \begin{pmatrix} 1 & 0 & 0 \\ 0 & \cos\theta & -\sin\theta \\ 0 & \sin\theta & \cos\theta \end{pmatrix} \begin{pmatrix} \eta_1 & 0 & 0 \\ 0 & \eta_2 & 0 \\ 0 & 0 & \eta_3 \end{pmatrix} \quad (4)$$

According to the definition of the invariant line, $(A - I)X = 0$, the rotation angle θ can be calculated to be:

$$\cos\theta = \frac{1 + \eta_3\eta_2}{\eta_3 + \eta_2} \quad (5)$$

"θ" (calculated to be 0.18°) is the rigid-body rotation angle to get invariant line after lattice deformation and defines the last orientation relationship between matrix and the precipitate. That is to say, "θ" is the angle of departure between the last O.R. and O.R. (Eq. (2)).

By linear algebra calculation, it is easy to get the eigenvalues and eigenvectors of the deformation matrix A [28]. For detailed calculation, see online Appendix A in Ref. [26]. All the results are shown in Table 2. The results show that one of eigenvalues always equals to 1 and corresponding eigenvector is the phase transformation invariant line. All the eigenvalues are real which make the precipitate possible to be bounded by three eigenplanes.

3.2.4. Prediction of the crystallography of the FCT → BCT precipitation

Based on the calculation above, the crystallographic characteristics of the FCT → BCT precipitation in $L1_0$-TiAl(Nb) alloy is listed in Table 3, which shows that the crystallographic features predicted by phase transforming invariant line theory are coincident well with those features measured by experiments. So, it is obviously that the invariant line theory is effective in the prediction of the crystallography of FCT → BCT precipitation in $L1_0$-TiAl(Nb) alloy.

According to the invariant line hypothesis, coherent needles lie on the cone of unextended lines as given by the stress-free transformation strain [29]. Any inextended line can be made an invariant line by the appropriate rotation. The coherent precipitate of γ_1 phase in this study was revealed to have a definite growth orientation of [001], which seems to derive that the distribution of coherent needles was restricted to [001] of the three [100] directions by FCT structure of the matrix. As a comparison, coherent Cr needles in Cu which are distributed on cones centered on the three ⟨100⟩ directions [30].

3.2.5. Morphology of the FCT → BCT precipitation

One can calculate precise elastic energy based on elastic constants of two phases in the precipitating system according to Khachaturyan [31]. However, the elastic constants are currently absent for phase γ_1-$Ti_4Al_3Nb_9$. It is found that precipitate dimensions tend to be inverse to the directional mismatch at the initial stage of a precipitation sequence [32] and could be predicted based on optimum matching at the interface [33]. The morphology of γ_1-$Ti_4Nb_3Al_9$ precipitating phase in Ti–Al–Nb alloy has been discussed roughly in the present author's work [11]. It is revealed that this precipitate takes a needle-like morphology, which coincides well with experimental observation.

There are three eigenvectors in Table 3 as a result of invariant line calculation. The rotation angle let the three real eigenvalues exist in this study. Luo and Weatherly implied that coherent inclusions tend to exhibit facets that are defined by unrotated directions (eigenvectors) of the transformation [25]. Thus we could deduce all the three eigenplanes bounding the precipitate phase shown as Fig. 5. The inclusion shape is predicted to be a parallelepiped with edges parallel to the eigenvectors and faces parallel to eigenplanes. The aspect ratio is inverse to the magnitude of the eigenstrains which is $|1 - n_3|/|1 - n_1| \cong 1/100$. That means the precipitate would take needle-like shape with a direction of [001]. The cross-sectional shape would be a parallelogram. The prediction coincides well with that of experimental observation.

As a comparison, the principle that precipitate dimensions tend to be inverse to the magnitude of the transformation strain [16] derived an elliptical cross-section. The proposal that interfaces are parallel to the planes of three independent dislocation loop arrays necessary to accommodate the transformation strain completely [34] would deduce that precipitate cross-sections normal to the invariant line direction have three distinct facets. The characterization of morphology and crystallography of the precipitate reaction in γ-TiAl/γ_1-$Ti_4Nb_3Al_9$ couple strongly support the postulate that precipitates are

Table 2
Theoretical eigenvalues, eigenvectors, invariant line and interfaces for $\gamma \rightarrow \gamma_1$ transforming in TiAlNb alloy

Phase transformation	Eigenvalues	Eigenvectors	Interfaces
$\gamma \rightarrow \gamma_1$	λ_1: 1.0000	V_1: [1,1.0779,21.0672]	F_1: (10.5335,10.5335,−1)
	λ_2: 1.00273	V_2: [10.3035,10.3071,1]	F_2: (26.5477, −26.6355,1)
	λ_3: 1.00277	V_3: [1,−0.9999,0.0037]	F_3: (1.0791,1,−21.4231)

Table 3
The theoretical and experimental crystallography of γ_1 phase

Phase transformation	Crystallographic characteristics	Theoretical values	Experimental values	Comparison
$\gamma \rightarrow \gamma_1$	O.R.	$(001)_\gamma//(001)_{\gamma_1}$; $[110]_\gamma 0.21^\circ \rightarrow [100]_{\gamma_1}$; $[\bar{1}10]_\gamma 0.21^\circ \rightarrow [100]_{\gamma_1}$	$(001)_\gamma//(001)_{\gamma_1}$; $[110]_\gamma//[100]_{\gamma_1}$; $[\bar{1}10]_\gamma//[100]_{\gamma_1}$	0.21°
	Habit plain	F_1: (10.5335,10.5335,−1)	(110)	3.8°
	Interface 2	F_2: (26.5477,−26.6355,1)	(1−10)	1.6°
	Interface 3	F_3:(1.0791,1,−21.4231)	(001)	3.8°
	Growing direction	[1,1.0779,21.0672]	[001]	3.7°

bounded by unrotated planes (eigenplanes) based on the experimental observation of three eigenplanes.

3.3. Morphology and crystallography of the γ_1-$Ti_4Al_3Nb_9$ equilibrium phase

The literature [10] and [11] have shown the same crystallography and morphology of the γ_1-$Ti_4Al_3Nb_9$ equilibrium phase in a $Ti_4Al_3Nb_9$ alloy. However, the direction of the phase takes ⟨111] compared with that of precipitated phase taking [001] revealed in this study. The departure of directions between them could also be explained well with invariant line theory. Dahmen [29] proposed that coherent needles lie on the cone of the unextended lines as given by the stress-free transformation strain while semicoherent needles lie along the intersection of the cone of unextended lines with a matrix slip plane.

Having established the lattice corresponding between matrix and precipitates, the coherent precipitated needles will grow further. Thus, the direction of the needle will be given by the solution of such simultaneous equations:

$$\begin{cases} aX + bY + cZ = 0 \\ X^2 + Y^2 + Z^2 = 1 \\ \eta_1^2 x^2 + \eta_2^2 y^2 + \eta_3^2 z^2 = 1 \end{cases} \quad (6)$$

where η_1, η_2 and η_3 are the main strain as showed in Eq. (1) and a, b, c are the index of the slip plane for the matrix. For $L1_0$ structure, the slip planes are {101}. Let $a = 1$, $b = 0$, $c = -1$, we can get the desired direction of the needle-like equilibrium phase as [0.579596, 0.572833, 0.579596] from Eq. (6). The departure angle between [111] and [0.579596, 0.572833, 0.579596] is 0.02°. It is shown that the theoretical result coincides well with the experimental result.

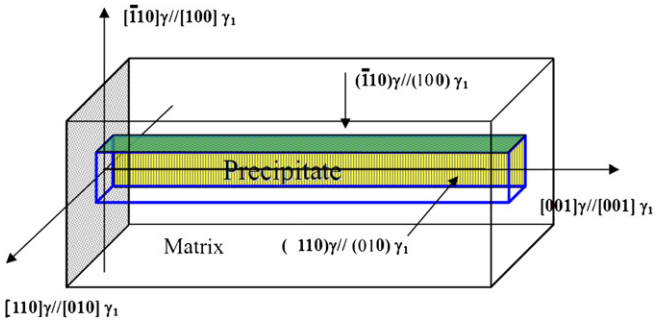

Fig. 5. A schematic showing the coherent precipitate is bounded by unrotated planes as well as the Bain orientation relationship between the matrix and the precipitate.

4. Conclusion

(1) After elongation of ageing time, the microstructure of the alloy consists of matrix γ-TiAl and needle-like precipitate γ_1-$Ti_4Nb_3Al_9$. The precipitates take needle-like shape with growing direction of [001], the cross-sectional shape of parallelogram and the Bain orientation relationship to $(001)_m//(001)_p$; $[110]_m//[100]_p$; $[\bar{1}10]_m//[100]_p$.
(2) The crystallographic features and morphology of the precipitate predicted by three-dimensional phase transforming invariant line theory coincides well with those measured by experiments.
(3) The needle direction of [001] at early stage for coherent precipitate γ_1-$Ti_4Nb_3Al_9$ and [111] for equilibrium phase γ_1-$Ti_4Nb_3Al_9$ could be explained well based on the invariant line theory.
(4) The characterization of morphology and crystallography of the precipitate reaction in γ-TiAl/γ_1-$Ti_4Nb_3Al_9$ couple sustain the postulate that precipitates are bounded by unrotated planes (eigenplanes) with edges parallel to the eigenvectors when three real eigenvalues exist.

Acknowledgement

This work was financially supported by Chinesisch-Deutsches Zeutrum fuer Wissenschaftsfoerderung, Beijing and Jiangsu Planned Projects for Postdoctoral Research Funds, China.

The authors would also like to greatly appreciate Dr. Chen G.L., Professor of Beijing University of Technology (PR China), for his constructive recommendation on the phase transformation of γ-TiAl → γ_1-$Ti_4Nb_3Al_9$ in $L1_0$-TiAl(Nb) alloys and to thank Dr. Liu Jiang-Wen, assistant Professor of South China University of Technology, for his help and enlightening discussion on the morphology of precipitation and the theory of the three-dimensional phase transformation invariant line.

References

[1] Yamaguchi M, Inui H, Ito K. Acta Mater 2000;48:307.
[2] Wang Yong, Wang JN, Yang Jie. J Alloys Compd 2004;364:93.

[3] Shagiev MR, Senkov ON, Salishchev GA, Froes FH. J Alloys Compd 2000;313:201.
[4] Gouma PI, Karadge M. Mater Lett 2003;57:3581.
[5] Noda T, Okabe M, Isobe S, Sayashi M. Mater Sci Eng A 1995;192/193:774.
[6] Tian WH, Nemoto M. Mater Sci Eng A 2005;329/331:653.
[7] Tian WH, Nemoto M. Intermetallics 1998;6:193.
[8] Hellwig A, Palm M, Inden G. Intermetallics 1998;6:79.
[9] Chen GL, Wang XT, Ni XQ, Hao SM, Cao JX, Ding JJ, et al. Intermetallics 1996;4:13.
[10] Chen GL, Wang JG, Ni XD, .Lin JP, Wang YL. Intermetallics 2005;13:329.
[11] Chen GL, Wang JG, Sun ZQ, Ye HQ. Intermetallics 1994;2:31.
[12] Liu HW, Yuan Y, Liu ZG, Liu J-M, Zhao XN, Zhu YY. Mater Sci Eng A 2005;412:328.
[13] Wechsler MS, Liberman DS, Read TA. Trans AIME 1953;197:1503.
[14] Bowles JS, Machenzie. Acta Metall 1954;2:129.
[15] Luo CP, Weatherly GC. Acta Metall 1989;37:791.
[16] Dahmen U. Scr Metall 1987;21:1029.
[17] Dahmen U. Acta Metall 1982;30:63.
[18] Aaroson HI. Metall Trans A 1993;24:241.
[19] Bollmann W. Philos Mag 1967;16:383.
[20] Zhang W-Z, Weatherly GC. Prog Mater Sci 2005;50:181.
[21] Zhang M-X, Kelly PM. Acta Mater 1998;46:4617.
[22] Kelly PM, Zhang M-X. Mater Forum 1999;23:41.
[23] Nie JF. Acta Mater 2004;5:795.
[24] Luo CP, Dahmen U. Acta Metall 1998;46:2063.
[25] Luo CP, Weatherly GC. Metall Trans 1988;19A:1153.
[26] Luo CP, Weatherly GC. Acta Metall 1987;35:1963.
[27] Liu HW, Yuan Y, Liu ZG, Liu J-M, Zhao XN, .Zhu YY. Scr Mater 2006;54(6):1087.
[28] Wayman CM. Introduction to the crystallography of martensitic transformations. Macmillan, New York: The Macmillan Company; 1964. p. 76–80.
[29] Dahmen U, Ferguson P, Westmacott KH. Acta Metall 1984;32:803.
[30] Weatherly GC, .Humble P, Borlan D. Acta Metall 1979;27:1815.
[31] Khachaturyan AG. Theory of structural transformations in solids. New York: Wiley; 1983.
[32] Dahmen U. Acta Mater 1982;30:63.
[33] Hall MG, Aaronson HI, Kinsman KR. Surf Sci 1972;31:257.
[34] Knowles CT, Clarebrough LM. Philos Mag 1989;59:637.